BIOCHEMISTRY
including biophysical chemistry & molecular biology
Article

Biochemistry **2010,** *49,* 3499–3509 3499
DOI: 10.1021/bi902073b

Glycal Formation in Crystals of Uridine Phosphorylase[†,‡]

Debamita Paul,[§] Seán E. O'Leary,[§,∥] Kanagalaghatta Rajashankar,[§,⊥] Weiming Bu,[§] Angela Toms,[§] Ethan C. Settembre,[§] Jennie M. Sanders,[§] Tadhg P. Begley,[∥] and Steven E. Ealick*[,§]

[§]*Department of Chemistry and Chemical Biology, Cornell University, Ithaca, New York 14853-1301,* [∥]*Department of Chemistry, Texas A&M University, College Station, Texas 77842, and* [⊥]*NE-CAT, Argonne National Laboratory, Argonne, Illinois 60439*

Received December 3, 2009; Revised Manuscript Received March 18, 2010

ABSTRACT: Uridine phosphorylase is a key enzyme in the pyrimidine salvage pathway. This enzyme catalyzes the reversible phosphorolysis of uridine to uracil and ribose 1-phosphate (or 2′-deoxyuridine to 2′-deoxyribose 1-phosphate). Here we report the structure of hexameric *Escherichia coli* uridine phosphorylase treated with 5-fluorouridine and sulfate and dimeric bovine uridine phosphorylase treated with 5-fluoro-2′-deoxyuridine or uridine, plus sulfate. In each case the electron density shows three separate species corresponding to the pyrimidine base, sulfate, and a ribosyl species, which can be modeled as a glycal. In the structures of the glycal complexes, the fluorouracil O2 atom is appropriately positioned to act as the base required for glycal formation via deprotonation at C2′. Crystals of bovine uridine phosphorylase treated with 2′-deoxyuridine and sulfate show intact nucleoside. NMR time course studies demonstrate that uridine phosphorylase can catalyze the hydrolysis of the fluorinated nucleosides in the absence of phosphate or sulfate, without the release of intermediates or enzyme inactivation. These results add a previously unencountered mechanistic motif to the body of information on glycal formation by enzymes catalyzing the cleavage of glycosyl bonds.

Uridine phosphorylase (UP;[1] EC 2.4.2.3) is a key enzyme in the pyrimidine salvage pathway, which when appropriate precursors are available provides an alternative to the energy-costly *de novo* biosynthetic pathway. UP catalyzes the reversible phosphorolysis of uridine (Urd) and 2′-deoxyuridine (dUrd) as well as their analogues to the respective nucleobases and ribose 1-phosphate (Scheme 1). UP is present in most organisms including prokaryotes, yeast, and higher organisms including mammals.

The three-dimensional structure of *Escherichia coli* UP (EcUP) has been previously studied in its unliganded form and in several complex forms (*1*−*4*). The structure of *Salmonella typhimurium* UP is very similar to that of EcUP (*5*). The bacterial enzyme exists as a hexamer comprised of six identical subunits. The protomer shares a common α/β fold with the nucleoside phosphorylase-I (NP-I) superfamily (*6*). Other members of this superfamily include mammalian (*7*, *8*) and bacterial (*9*) purine nucleoside phosphorylases (PNPs), mammalian and bacterial methylthioadenosine phosphorylases (*10*), *S*-adenosylhomocysteine/methylthioadenosine nucleosidase (*11*), and AMP nucleosidase (*12*). Despite the differences in amino acid sequence, oligomeric state, and substrate specificity, the enzymes of this superfamily are characterized by a common topology.

In mammalian cells two isoforms of UP have been identified (*13*). The class 1 isozyme is more widely distributed and has been studied in detail. The class 2 isozyme shows a broader substrate specificity and substantial differences in tissue-specific expression. Recently, the structure of class 1 human UP (hUP) was reported in unliganded and ligand-bound forms (*14*). The human enzyme exists as a dimer with the same structural fold as the bacterial enzyme. Nearly all active site residues are conserved between the mammalian and bacterial homologues and show similar protein−ligand interactions. Structural analogy of UP to the closely related PNP, which has been studied extensively by isotope effects, theoretical methods, and inhibition experiments (*15*−*17*), suggests that the chemical reaction proceeds via an oxocarbenium ion intermediate (**3**, Scheme 1).

Carbenium ions have fascinated organic chemists for almost a century, and the properties of this important class of reactive intermediates have been studied extensively (*18*). In addition to the nucleoside phosphorylase reaction, carbenium ions have been proposed as intermediates in several enzyme-catalyzed reactions, including the prenyl transfer and cyclization reactions involved in terpene biosynthesis (*19*), the pyrrole tetramerization involved in porphyrin biosynthesis (*20*), the glycosyl transfer reactions

[†]This work was supported by NIH Grants GM073220 to S.E.E. and DK44083 to T.P.B. This work is based upon research conducted at the Advanced Photon Source on the Northeastern Collaborative Access Team beamlines, which are supported by award RR-15301 from the National Center for Research Resources at the National Institutes of Health. Use of the Advanced Photon Source is supported by the U.S. Department of Energy, Office of Basic Energy Sciences, under Contract No. DE-AC02-06CH11357.

[‡]The coordinates for the UP structures have been deposited in the Protein Data Bank under accession numbers 3KVV, 3KU4, 3KVY, 3KVR, and 3KUK for EcUP/FUra/glycal/sulfate, bUP, bUP/Ura/glycal/sulfate, bUP/FUra/deoxyglycal/sulfate, and bUP/dUrd/sulfate, respectively.

*To whom correspondence should be addressed. Telephone: (607) 255-7961. Fax: (607) 255-1227. E-mail: see3@cornell.edu.

[1]Abbreviations: UP, uridine phosphorylase; EcUP, *Escherichia coli* uridine phosphorylase; bUP, bovine uridine phosphorylase; hUP, human uridine phosphorylase; PNP, purine nucleoside phosphorylase; NP, nucleoside phosphorylase; Ura, uracil; FUra, 5-fluorouracil; Urd, uridine; FUrd, 5-fluorouridine; FdUrd, 5-fluoro-2′-deoxyuridine; dUrd, 2′-deoxyuridine; SeMet, selenomethionine; IPTG, isopropyl 1-β-D-galactopyranoside; MES, 2-(*N*-morpholino)ethanesulfonic acid; Tris, tris(hydroxymethyl)aminomethane; DTT, dithiothreitol; TEV, tobacco etch virus; PEG 5 K MME, polyethylene glycol 5K monomethyl ether; APS, Advanced Photon Source; SAD, single wavelength anomalous diffraction; NCS, noncrystallographic symmetry.

Published on Web 04/05/2010

Scheme 1

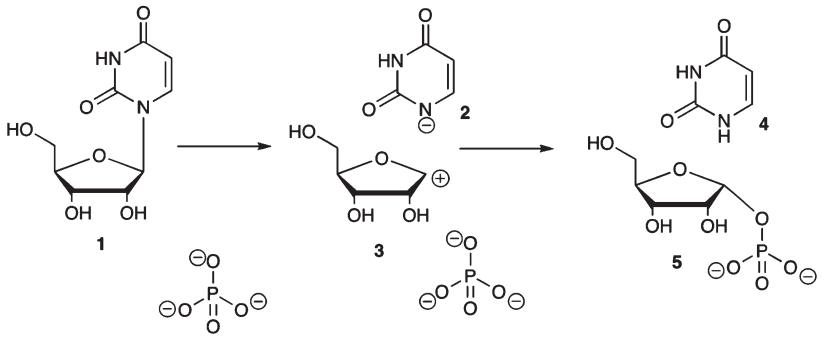

involved in a wide variety of glycosylations (*21*), and the thiazole/pyrimidine coupling reaction involved in thiamin phosphate formation (*22*, *23*). With the exception of the latter reaction, evidence for enzyme-bound carbenium ions is always indirect, relying on substituent and isotope effects, on intermediate trapping, and on inhibition studies. A possible exception comes from studies on human CD38 (*24*).

Here we present the crystal structures of EcUP incubated *prior to crystallization* with 5-fluorouridine (FUrd) and sulfate and of bovine UP (bUP) treated with 5-fluoro-2′-deoxyuridine (FdUrd) or Urd, and sulfate. Unexpectedly, the electron density for each structure shows three separate species corresponding to uracil (Ura) or 5-fluorouracil (FUra), sulfate, and a ribosyl species, which was modeled as a UP-bound glycal or deoxyglycal. Our studies also include the determination of the structure of unliganded bUP and bUP treated with dUrd and sulfate. In the latter structure the dUrd is not cleaved.

MATERIALS AND METHODS

Chemical Reagents. M9 minimal medium, L-amino acids, magnesium sulfate, calcium chloride, Ura, FUra, Urd, FUrd, dUrd, and FdUrd were purchased from Sigma-Aldrich. Ni-NTA resin was obtained from Qiagen (Valencia, CA), MEM vitamin solution was from Invitrogen, ampicillin, MES, ferrous sulfate, and L-selenomethionine (SeMet) were from Acros, and glucose was from Fisher.

Crystallization of EcUP. EcUP was expressed and purified as previously described (*1*). EcUP was crystallized by the hanging drop method using 2 μL of protein solution plus 1 μL of well solution. The protein crystallized under conditions very similar to those published by Burling et al. (*2*). The crystals grew best at 22 °C with the optimized mother liquor conditions of 5%−7% PEG 4K, 0.1 M 2-(*N*-morpholino)ethanesulfonic acid (MES) pH 6.2−6.3, and 5% glycerol. Crystals grew over 2 days to a maximum size of ~300 μm × 300 μm × 200 μm. For complex crystallization, the protein was incubated with 10 mM FUrd and 10 mM ammonium sulfate at 4 °C for 12 h prior to crystallization. Cocrystals grew within 2 days, under similar conditions as the unliganded form. These crystals were rodlike with maximum dimensions of 25 μm × 25 μm × 500 μm.

Cloning of bUP. The bUP gene was amplified from the cDNA clone Mbov3 139P15 (BacPac, http://bacpac.chori.org/) by PCR with the following primer pair: 5′-CTG TAC TTC CAG GGT ATG GCC TCC ACC GCG GCT GAA ACG GAG-3′ and 5′-GAA AGC TGG GTG TCA GGC CTG CAT CAG GCG CTT C-3′. The PCR product was then used as a template for another round of thermocycling with the following primers designed to add AttB sites to the ends of the encoded protein: 5′-G GGG ACA AGT TTG TAC AAA AAA GCA GGC TCC GGA AAT CTG TAC TTC CAG-3′ and 5′-GGG GAC CAC TTT GTA CAA GAA AGC TGG GTG-3′. The PCR product was purified and used in a Gateway BP recombination reaction with the Invitrogen vector pDONR221 following the manufacturer's instructions. Clones were screened by restriction digest and verified by sequencing. A correct clone was used in a Gateway LR recombination reaction with the plasmid pDESTF1, which is a gateway-adapted vector based on the pET system from Novagen. The plasmid pDESTF1 encodes an N-terminal 6×His tag and is under the control of the T7*lac* promoter, which is a hybrid promotor having a T7 promotor sequence followed by a *lac* operator sequence. Again, clones were screened by restriction digest. A correct clone was named pBovUP.XF1.

Expression and Purification of bUP. The plasmid pBovUP.XF1 was transformed into BL21Star(DE3) *E. coli*. An overnight culture of 10 mL was grown in Luria−Bertani media at 37 °C supplemented with 100 μg/mL ampicillin and then diluted into 1 L of medium containing 100 μg/mL ampicillin. The cells were grown at 37 °C until they reached an OD_{600} of 0.4, and the temperature was then reduced to 20 °C. The cells were induced with 1 mM isopropyl 1-β-D-galactopyranoside (IPTG) when the OD_{600} reached 0.6 and allowed to grow overnight at 15 °C. Cells were harvested by centrifugation at 9000*g* for 10 min at 4 °C and stored at −20 °C.

The frozen cell pellet was resuspended in 50 mL of lysate buffer (50 mM tris(hydroxymethyl)aminomethane (Tris), pH 8.0, 300 mM NaCl, 10 mM imidazole, 1 mM dithiothreitol (DTT)), and cells were subjected to sonication. Cell debris was removed by centrifugation at 35000*g*, and the clear lysate was loaded onto a Ni-NTA column preequilibrated with the lysate buffer. After the lysate was loaded, the column was washed with wash buffer (50 mM Tris, pH 8.0, 300 mM NaCl, 30 mM imidazole, 1 mM DTT) for about 1 h. Pure protein was eluted with 50 mM Tris, pH 8.0, 300 mM NaCl, 250 mM imidazole, and 1 mM DTT. The recombinant protein was subjected to tobacco etch virus (TEV) protease digestion, to remove the hexahistidine tag, in a buffer containing 50 mM Tris, pH 8.0, 150 mM NaCl, and 1 mM DTT for 12 h. After the completion of proteolysis, as judged by SDS−PAGE analysis, the protein was reloaded onto a Ni-NTA column, and the flow-through was collected. The nonbinding material was then buffer exchanged into 20 mM Tris, pH 8.0, and 150 mM NaCl. The protein was then concentrated to 3 mg/mL using an Amicon Ultra centrifugal device with a 30 kDa MWCO (Millipore). The protein was estimated to be greater than 95% pure based on SDS−PAGE analysis. The pure protein was flash frozen and stored at −80 °C.

Expression and Purification of SeMet bUP. The expression of SeMet-incorporated protein involved some modifications

Table 1: Data Collection Statistics for UP Crystals[a]

	EcUP/FUra/glycal/SO_4	SeMet bUP	bUP	bUP/FUra/deoxyglycal/SO_4	bUP/Ura/glycal/SO_4	bUP/dUrd/SO_4
resolution (Å)	2.2	3.5	2.1	2.6	2.3	2.8
space group	$P3_2$	$I4_122$	$P4_1$	$P4_12_12$	$P4_12_12$	$P4_12_12$
a (Å)	92.9	81.9	74.1	82.4	83.5	82.6
c (Å)	145.0	266.3	266.9	258.6	260.1	259.0
no. of ASU	6	1	4	2	2	2
Matthews no. (Å^3/Da)	2.28	3.18	2.62	3.13	3.23	3.02
solvent content (%)	43.3	60	52	60	61	59.4
unique reflections	68027	10857	91922	28368	41493	20780
redundancy	7.5	8.5	2.2	6.1	7.0	3.1
completeness	99.3 (99.0)	98.9 (98.5)	95.7 (95.1)	99.5 (95.8)	100 (99.9)	89 (73.8)
R_{sym}[b] (%)	4.0 (9.6)	9.4 (34.4)	9.1 (36.3)	11.4 (36.4)	20.8 (54.9)	11.4 (21.3)
I/σ	17.9 (4.6)	11.1 (2.4)	12.4 (2.7)	20.6 (3.6)	35.0 (6.14)	9.5 (2.5)

[a]Values for the highest resolution shell are given in parentheses. [b]$R_{sym} = \sum\sum_i |I_i - \langle I \rangle| / \sum \langle I \rangle$, where $\langle I \rangle$ is the mean intensity of the N reflections with intensities I_i and common indices h,k,l.

to the native protein expression protocol. The plasmid pBovUP.XF1 was transformed into methionine-auxotrophic B834(DE3) *E. coli*. A 50 mL starter culture in M9 minimal medium, containing 40 mg/mL L-amino acids, 0.4% glucose, 2 mM magnesium sulfate, 1% MEM vitamin solution, 0.1 mM calcium chloride, 25 μg/mL ferrous sulfate, and 100 μg/mL ampicillin, was inoculated with a single colony and grown overnight at 37 °C. The starter culture was grown in the presence of L-methionine to give a healthy start, as selenomethionine is poisonous to cells. The starter culture was then used to inoculate 1 L of M9 minimal medium having the same composition but L-selenomethionine in place of L-methionine. The starter cells were washed with the M9 minimal media prior to inoculation to remove the normal methionine. Induction was done using 1 mM IPTG at OD_{600} of 0.6 for 12−16 h at 15 °C. Cells were harvested by centrifugation at 9000*g*. The purification process was the same as that for the native protein. The pure protein was stored in 20 mM Tris, pH 8.0, 150 mM NaCl, and 1 mM DTT. For the native protein, 1 L of cell culture produced about 20 mg of pure protein, while for the SeMet protein, only ~4 mg of pure protein was obtained from 1 L of culture.

Crystallization of bUP. Initial crystallization conditions of unliganded bUP were determined using sparse matrix screens Crystal Screen 1 and 2 (Hampton Research) at 22 °C using the hanging drop vapor diffusion technique. Several conditions yielded thin needle crystals that varied in quality. The optimized conditions were 100 mM MES (pH 6.3), 140 mM ammonium sulfate, and 18% PEG 5K monomethyl ether (PEG 5K MME). The crystals grew in 3−5 days to the size of ~200 μm long rods. Drops containing 1 μL of protein and 1 μL of reservoir solution were optimal for crystal growth.

To obtain the ligand complexes, the enzyme was separately incubated with 5 mM each of Urd, dUrd, or FdUrd and 5 mM ammonium sulfate for 12 h prior to crystallization. The rod-shaped 200−300 μm long crystals of the substrate complexes were obtained under very similar conditions (0.1 M MES, pH 6.0−6.5, 0.2 M ammonium sulfate, 18−25% PEG 5K MME). SeMet bUP crystals were grown by hanging drop vapor diffusion at 22 °C using a well solution containing 100 mM MES (pH 6.0), 1 M LiCl, and 20% PEG 6K. In this case the needle-like crystals were ~50−80 μm long and attained their maximum size in 4−6 days.

Data Collection and Processing. The data for the EcUP complex were measured at beamline 8-BM at the NE-CAT beamline at the Advanced Photon Source (APS) at Argonne National Laboratory using a Quantum 315 detector (Area Detector Systems Corp.). Data were processed using DENZO and SCALEPACK (*25*). The data for native bUP, SeMet bUP, and the complexes were collected at the 24-ID-C station of the NE-CAT beamline at the APS also using a Quantum 315 detector. A cryoprotectant solution of 10%−20% glycerol in the mother liquor was used to avoid damage during freezing. The data were indexed, integrated, and scaled using the HKL2000 program suite (*25*). The data collection and data processing statistics are shown in Table 1.

Structure Determination and Refinement of the EcUP/Ura/Glycal/Sulfate Complex. The current structure was determined by molecular replacement using the program CNS (*26*) with the previously reported native UP monomer structure (Protein Data Bank entry 1LX7) as the search model (*2*). The refinement procedure included successive rounds of rigid body refinement, simulated annealing refinement, temperature factor refinement, and model building. A composite omit map was examined to determine the active site contents and to identify alternate conformations of side chains. Side chains and regions showing poorly defined peptide backbone electron density were then manually adjusted using the program O (*27*). Noncrystallographic symmetry (NCS) restraints improved density for some of the weaker regions. The active site ligands were clearly observed in the $F_o - F_c$ maps, but ligand models were not included in the refinement until later steps to minimize model bias. After all protein atoms were refined, the appropriate ligand models were manually fit into the active site, followed by a few cycles of refinement. The model was examined using CNS and PROCHECK (*28*). The final refinement statistics are summarized in Table 2.

Structure Determination and Refinement of bUP in Unliganded and Complex Forms. To determine the structure of bUP, the single wavelength anomalous diffraction (SAD) method was used. Ten Se sites out of the 12 possible sites were found by the program SHELXD (*29*). SAD phasing was done by the maximum likelihood program MLPHARE (*30*), and finally a density-modified map was calculated using the program SHARP (*31*), which was used for initial model building at 3.5 Å. Manual model building was done using the interactive graphic program Coot (*32*). After a few rounds of model building, a biologically relevant crystallographic dimer in the SeMet UP unit cell was identified and used as the starting model for molecular replacement with the higher resolution (2.1 Å) native data set. Molecular replacement was carried out, with the dimer as starting

Table 2: Refinement Statistics and Model Building for UP Data Sets

	EcUP/FUra/glycal/SO_4	bUP	bUP/FUra/deoxyglycal/SO_4	bUP/Ura/glycal/SO_4	bUP/dUrd/SO_4
resolution (Å)	2.2	2.1	2.6	2.3	2.8
no. of protein atoms	10879	8862	4487	4483	4489
no. of water molecules	839	980	155	334	77
no. of ligand atoms	138	20	44	54	42
rmsd from ideal geometry bonds (Å)	0.018	0.008	0.008	0.008	0.007
angles (deg)	1.980	1.141	1.173	1.128	1.019
R factor[a] (%)	19.7	17.9	16.7	18.0	18.2
R_{free}[b] (%)	23.9	22.5	20.5	20.8	25.0
Ramachandran plot					
most favored regions (%)	89.4	93.2	91.1	91.8	88.9
additionally allowed regions (%)	10.2	6.8	8.9	8.2	11.1
generously allowed regions (%)	0.4	0.0	0.0	0.0	0.0
disallowed regions (%)	0.0	0.0	0.0	0.0	0.0

[a] R factor $= \sum_{hkl}||F_o| - k|F_c||/\sum_{hkl}|F_o|$, where F_o and F_c are observed and calculated structure factors, respectively. [b] For R_{free} the sum is extended over a subset of reflections (5%) excluded from all stages of refinement.

model, using CNS (*33*), and the second dimer was found by translational search after fixing the first one in the unit cell. Initial electron density maps were further improved by 4-fold NCS averaging with the RAVE suit of programs (*34*). The refinement procedure involved successive rounds of rigid-body refinement, simulated annealing refinement, temperature factor refinement, and model rebuilding. Initial refinement cycles were performed using CNS and final rounds with the PHENIX suite of programs (*35*). The bUP complex structures were determined by molecular replacement using CNS with the refined native bUP dimer as the search model. The active site contents and alternative side chain conformations were determined using $F_o - F_c$ and composite omit electron density maps. Tight NCS restraints were applied during initial rounds of refinement to improve density in the weaker regions and were slowly relaxed during the final rounds of refinement. The parameter and topology files for the ligands were generated using the Dundee PRDRG2 server (*36*). The sulfate ions and water molecules were added and refined in CNS. The refinement statistics are summarized in Table 2.

Analytical Ultracentrifugation. Analytical ultracentrifugation was used to determine the oligomeric states of EcUP and bUP. The software package DCDT+ (*37*) was used for data analysis. The basic principle involves a time derivative approach for sedimentation velocity analysis. The sedimentation coefficient distribution function is fitted to a Gaussian curve to determine concentration, sedimentation coefficient, and diffusion coefficient of a particular species. However, the molecular weight determination also requires the density of the solvent, the partial specific volume of the protein, the viscosity of the solvent, and its temperature dependence in order to account for the effect of temperature and solvent on sedimentation property. The program Sedenterp (*38*) was used for the calculation of those properties.

^{1}H NMR Spectroscopy of EcUP-Catalyzed FUrd Hydrolysis in the Presence and Absence of Sulfate. ^{1}H NMR spectra were obtained using a Varian INOVA 600 MHz spectrometer and a Varian H{C/N} probe equipped with triple-axis pulsed field gradients. A solution (0.5 mL) was prepared containing sodium sulfate (60 mM) and FUrd (10 mM) in 50 mM ammonium acetate buffer (prepared with D_2O, pD 7.4). After addition of UP (0.25 mL, final concentration 140 μM), the field-frequency lock and magnet *Z*-shims were quickly optimized. Sixty spectra were then acquired at 81 s intervals, followed by a further 11 spectra acquired at 10 min intervals. Each final spectrum was produced by averaging 16 transients. The intervals between acquisition of the spectra were determined by appropriately arraying the preacquisition delay. The residual solvent resonance was suppressed by presaturation. Resonances corresponding to the C6-H nuclei of FUrd and FUra were integrated for the individual spectra and used to determine the concentration of the substrate and product as a function of reaction time. The concentrations were calculated at the individual time points as the product of the initial substrate concentration and the integral value of substrate or product expressed as a fraction of the total integral value for the two species; no side products were observed during the reaction. The identity of the FUra product was established by comparison of its ^{1}H NMR spectrum with that of a commercially available standard. FUrd and bUP were present at concentrations of 5 and 0.01 mM, respectively.

^{1}H NMR Spectroscopy of bUP-Catalyzed FUrd Hydrolysis in the Presence and Absence of Sulfate. NMR spectra were acquired on a Varian INOVA 600 MHz instrument equipped with a Varian H{C/N} inverse-detection probe and triple-axis pulsed field gradients. The residual HDO resonance was suppressed by presaturation. Immediately prior to the experiment, the enzyme was buffer-exchanged into a freshly prepared buffer composed of 0.1 M ammonium bicarbonate and 0.15 M sodium chloride in D_2O (pD 7.1). For observation of the time course of the hydrolysis reaction, the enzyme was added to a solution of FUrd (5 mM) in the same buffer. In a second experiment, potassium sulfate was also included at a final concentration of 5 mM prior to the addition of enzyme. The final enzyme concentration was ~10 μM. After mixing the enzyme and substrate solutions, the instrument shims were optimized, and the time course of the reaction was followed by acquiring 30 traces at intervals of 3 min over 1.5 h. Each trace was generated from an average of 32 transients. The spectra were processed by applying exponential multiplication (0.35 Hz) to the free induction decay prior to Fourier transformation.

Figure Preparation. All figures were prepared using ChemDraw and PyMOL (*39*).

RESULTS

Observation of an Unexpected Species in the Active Sites of EcUP and bUP. The active sites of EcUP treated with FUrd and sulfate, of bUP treated with FdUrd and sulfate, and of bUP

treated with Urd and sulfate showed three distinct species (Figure 1a−c). The three species were well separated and corresponded to Ura (or FUra), sulfate, and a ribosyl species which we model as a glycal. The structure of bUP treated with dUrd and sulfate showed uncleaved nucleoside (Figure 1d).

Structure of the EcUP/FUra/Gycal/Sulfate Complex. The three-dimensional structure of EcUP has been previously well characterized (Figure 2a,b) including the identification of key active site residues (*1*−*4*). The active site of the enzyme can be divided into base, sugar, and phosphate binding sites (Figure 3a). In the EcUP complex, the sites are occupied by FUra, glycal, and sulfate, respectively. The binding site of sulfate is nearest to the protein surface and involves side chain interactions with Arg30, Arg91, and Thr94 from one subunit and Arg48 from the neighboring subunit. Thr94 and Gly26 are involved in phosphate binding via main chain interactions. The 5-hydroxyl group of the glycal is stabilized by a hydrogen-bonding interaction with $N^{\varepsilon 2}$ of His8 coming from the other adjacent monomer and an active site water molecule. The 3-hydroxyl group of the glycal is stabilized by a hydrogen bond with the side chain of Glu198. The O4 of FUra is hydrogen bonded to Arg168 and an active site water molecule that is in turn hydrogen bonded to Arg223. O2 and N3 form hydrogen bonds with the side chain of Gln166. The FUra is also involved in a herringbone stacking interaction with Phe162. The 5-fluoro substituent of FUra is located in a hydrophobic pocket composed of residues Ile220 and Val221.

Structure of bUP. The basic fold of the nucleoside phosphorylase-I superfamily is conserved in bUP (Figure 2d). The characteristic feature of the superfamily is a centrally located β-sheet, which forms a distorted β-barrel, surrounded by several α-helices. The overall fold is highly similar to the recently published structure of hUP (*14*). The sequence similarity between the human and bovine enzymes is 80%. The overall three-dimensional structures are also similar, with an rmsd of 0.8 Å for 289 residues, and both enzymes are homodimers in the crystal structures. The dimer (Figure 2c) has a globular shape with dimensions of 65 × 40 × 25 $Å^3$. Each homodimer contains two active sites located at the dimer interface and utilizing residues from both chains. The dimer interface mostly includes the N-terminal end of one chain, consisting of residues 20−24, and a loop region of the other chain, containing residues 220−224.

Structures of bUP Complexes. The active site residues of bUP are very similar to those of hUP (*14*). In the current study, structures of three bUP complexes were determined: bUP/FUra/deoxyglycal/sulfate, bUP/Ura/glycal/sulfate, and bUP/dUrd/sulfate (Figure 3b−d).

As was the case for EcUP, the sulfate binding site is more exposed to the surface than either the base or sugar binding sites. The residues involved in sulfate binding are Gly59, Arg137, and Thr140 from one subunit and Arg93 from the other. The sulfate ion forms hydrogen bonds with the side chains of Arg137 and Arg93, the amide nitrogen atom of Gly59, and both the side chain and amide nitrogen atoms of Thr140. Arg63 forms a hydrogen bond with sulfate in only the bUP/FUra/deoxyglycal/sulfate complex, but the density is very weak in the other two complexes, suggesting that the side chain is disordered.

The most interesting aspect of the current study is the observation of glycals in two of the bUP complexes. The glycal site is sandwiched between the Ura (FUra) and sulfate binding sites in the bUP/FUra/deoxyglycal/sulfate and bUP/Ura/glycal/sulfate complexes. The side chain of Glu249 forms a hydrogen bond with the 3-hydroxyl group of the ribose ring.

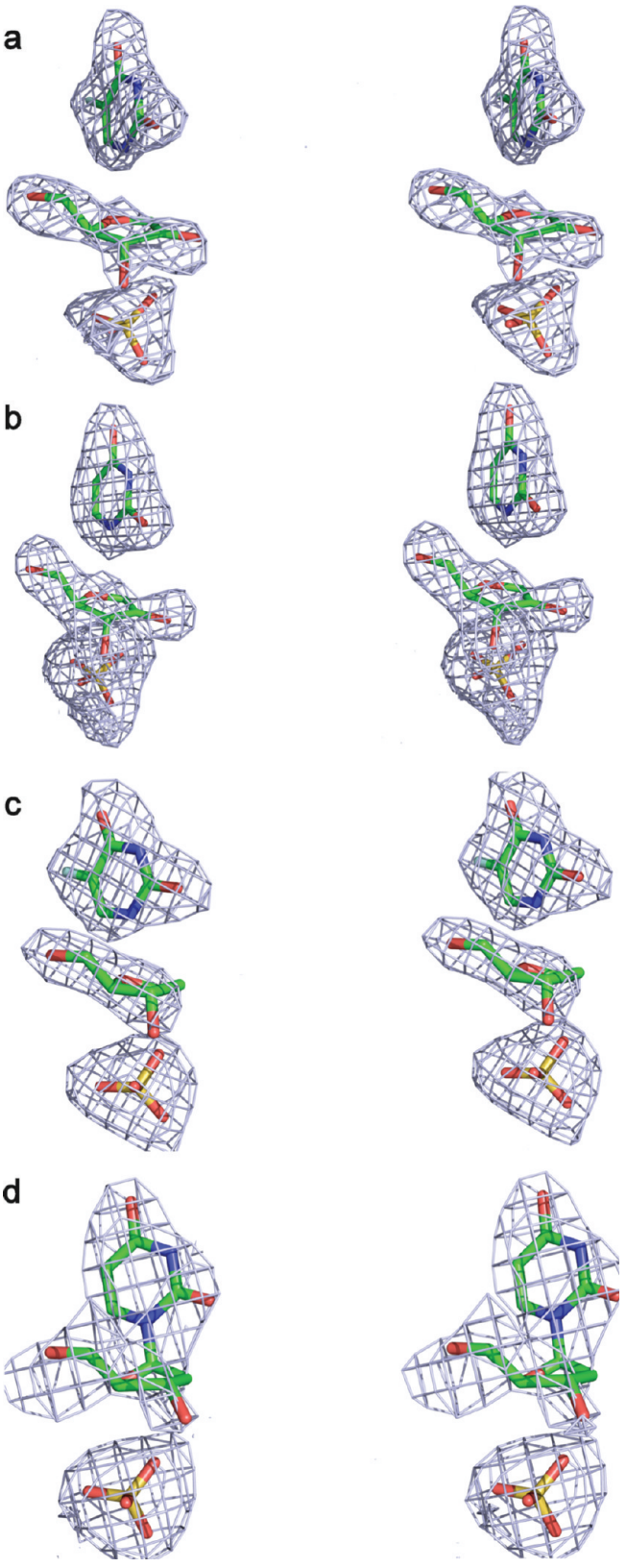

FIGURE 1: Electron density for EcUP and bUP complexes. (a) Stereoview of the active site electron density for the EcUP/FUra/glycal/sulfate complex. (b) Stereoview of the active site electron density for the bUP/Ura/glycal/sulfate complex. (c) Stereoview of the active site electron density for the bUP/FUra/deoxyglycal/sulfate complex. (d) Stereoview of the active site electron density for the bUP/dUrd/sulfate complex. All $F_o - F_c$ electron density maps are contoured at 3σ. C atoms are colored in green, N atoms in blue, O atoms in red, and S atoms in yellow.

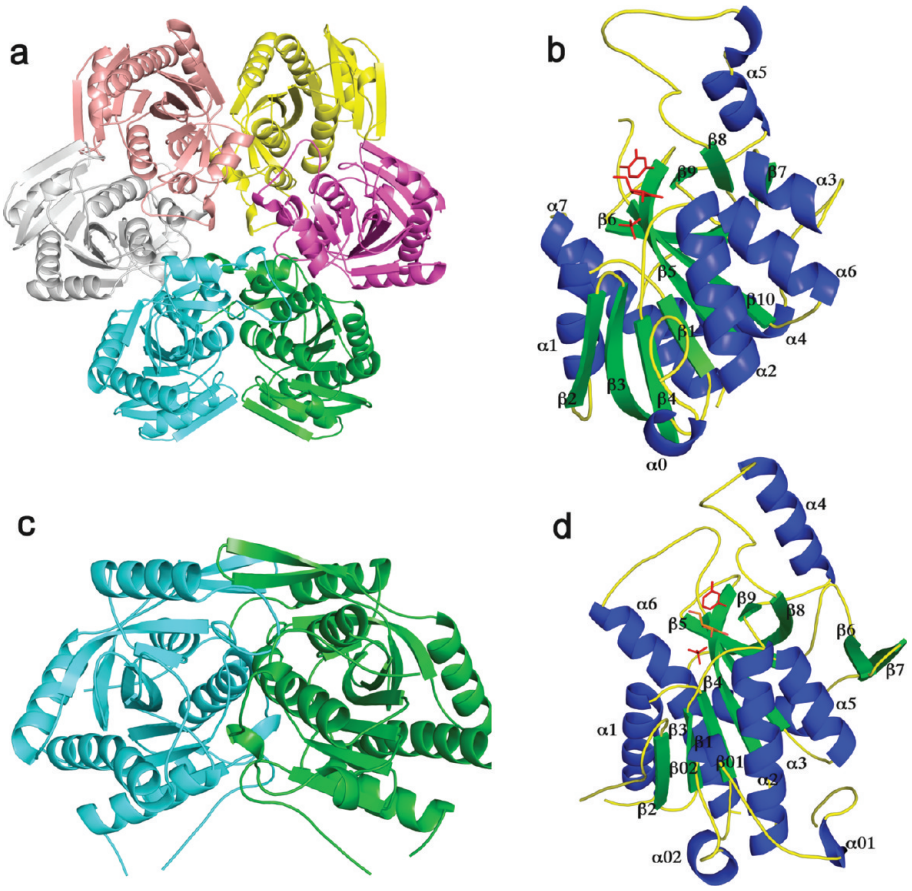

FIGURE 2: Structures of EcUP and bUP. (a) Cartoon representation of the EcUP hexamer color coded by monomer. (b) Cartoon representation of the EcUP monomer color coded by secondary structure. (c) Cartoon representation of the dimer of bovine UP color coded by monomer. (d) Cartoon representation of the monomer of bUP colored by the secondary structural elements. The α-helices are colored in blue, *β*-strands are colored in green, and the loops are colored in yellow. The ligands are represented as stick models and are shown in red.

The 5-hydroxyl group hydrogen bonds with $N^{\varepsilon 2}$ of His35 coming from the adjacent monomer. An active site water molecule also makes a hydrogen bond with the 5-hydroxyl group. The ribosyl moiety in the bUP/dUrd/sulfate complex utilizes the same interactions with the residues as the glycal.

The Ura (FUra) binding site of the enzyme is located in the cleft between two monomers and is comparatively less exposed to the surface. In the active site, the O4 atom of Ura forms a hydrogen bond with Arg218 and an active site water molecule that is in turn hydrogen bonded to Arg274. Residue Gln216 forms hydrogen bonds with O2 and N3 of the pyrimidine. Phe212 forms herringbone packing interactions with the pyrimidine. The 5-substituent of FUra inserts into a pocket formed by the side chains of Leu271 and Leu272. The side chain of Ile280 is also near this hydrophobic pocket. After glycal formation, O2 of the Ura/FUra would be protonated. However, tautomerization would result in the keto tautomer of uracil, which is more stable at the crystallization pH (6−6.5). Consequently, the keto form was modeled into the density, and the side chain orientation of Gln216 is determined accordingly.

Second Sulfate Binding Site. The $F_o - F_c$ electron density map in the UP/Urd/sulfate complex structure shows a large peak suggesting the possibility of a second substrate binding site. This site is located near the surface and exposed to the solvent ion channel. The main interaction involves hydrogen bonds with several water molecules, along with Tyr126, His127, and His129. Because the crystallization conditions included high sulfate concentrations, this site may be an artifact of crystallization.

Analytical Ultracentrifugation Results. Table 3 shows the results of the data analysis. The analytical ultracentrifugation data show that bUP exists as a dimer in solution whereas the EcUP is a hexamer.

Steady-State Reaction of the UP Enzymes with FUrd under Crystallization Conditions. Observation by ^{1}H NMR of the reactions of FUrd catalyzed by bUP and EcUP in the presence and absence of sulfate demonstrated that, under the conditions used for incubation of the enzymes with fluorinated nucleosides and sulfate prior to crystallization, most of the nucleoside was hydrolyzed regardless of whether sulfate was present (Figure 4). EcUP was also capable of catalyzing the hydrolysis of Urd at a considerably slower rate than for FUrd (data not shown). We could not detect the accumulation of any products except for FUra and the four anticipated isomers of D-ribose (limit of detection ~5%). Our enzyme preparations removed phosphate from the protein, and the NMR spectra showed no accumulation of ribose 1-phosphate. Furthermore, the NMR signals for the anomeric protons of the four ribose isomers were doublets, indicating that solvent-derived deuterium was not incorporated at the C2 position of the sugar on the time scale of the experiment. This suggests that glycal formation does not occur in the UP-catalyzed steady-state hydrolysis of 5-fluorouridine under the conditions employed.

DISCUSSION

Crystal Packing for bUP. The crystal structures of unliganded, complexed, and SeMet bUP show an interesting

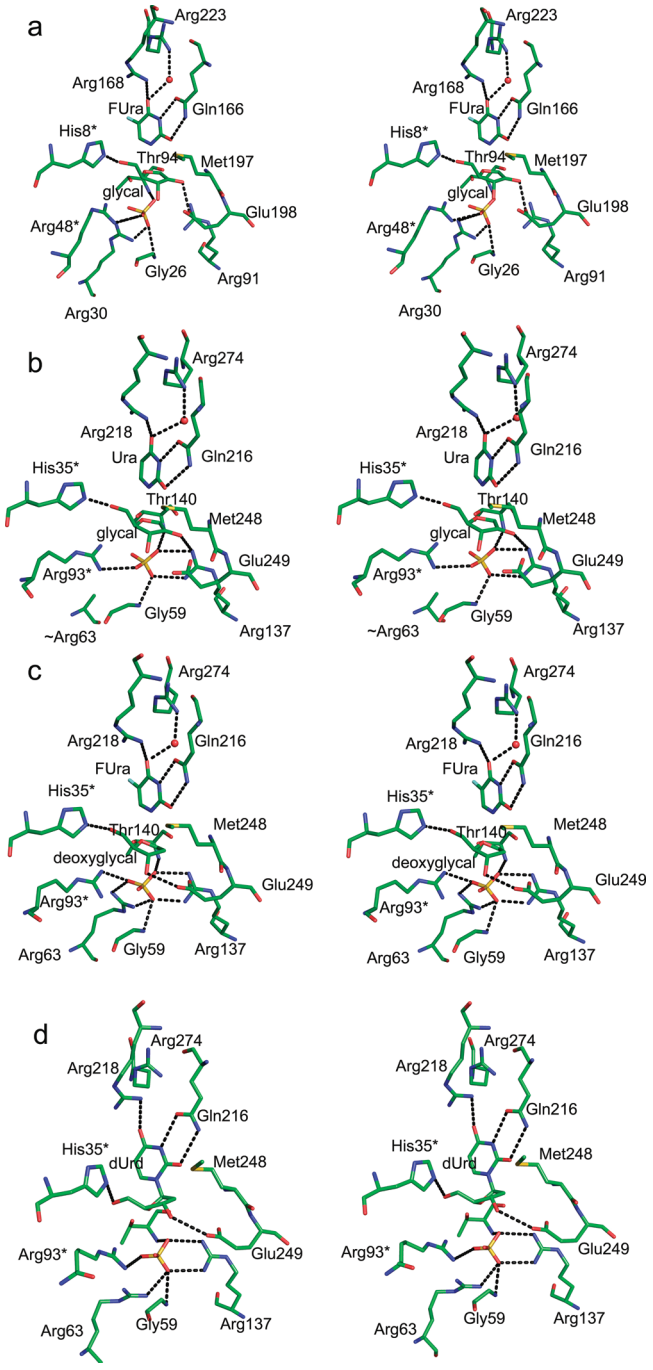

FIGURE 3: Active sites of EcUP and bUP. (a) Stereoview of the active site of the EcUP/FUra/glycal/sulfate complex. (b) Stereoview of the active site of the bUP/Ura/glycal/sulfate complex. (c) Stereoview of the active site of the bUP/FUra/deoxyglycal/sulfate complex. (d) Stereoview of the active site of the bUP/dUrd/sulfate complex. Important surrounding residues are shown in stick representation. C atoms are colored in green, N atoms in blue, O atoms in red, and the S atom in yellow.

variation in crystal packing. While all of the crystals belong to the tetragonal crystal system and have similar unit cell dimensions, three different space groups are represented (Table 1); however, the dimeric bUP structure remains intact in all of the three space groups. In the SeMet bUP (space group $I4_122$), the asymmetric unit is a monomer, and the crystallographic 2-fold axes generate the dimers. In the bUP complex structures (space group $P4_12_12$), the asymmetric unit contains one complete dimer. The unliganded structure (space group $P4_1$) has two complete dimers in the asymmetric unit. For the lower symmetry cases, the NCS mimics the crystallographic symmetry of the highest symmetry space group.

Table 3: Analytical Ultracentrifugation

		molecular mass (kDa)		
sample[a]	concn (mg/mL)	measured	calcd	oligomeric state
EcUP	2.0	181.89	163	hexamer
EcUP	1.0	176.26	163	hexamer
bUP	0.5	62.89	68	dimer

[a]The samples were buffer exchanged in 20 mM Tris (pH 7.0) and 150 mM NaCl.

Conformational Differences between Unliganded and Complexed bUP. The present studies report the structures of unliganded bUP and the bUP/FUra/deoxyglycal/sulfate, bUP/Ura/glycal/sulfate, and bUP/dUrd/sulfate complexes. Comparisons of the bUP structures show conformational changes upon ligand binding (Figure 5). Conformational changes were also reported for hUP upon inhibitor binding (*14*). Substrate binding is associated with movement of a loop region (277−286), which forms a lid over the active site and results in a "closed" conformation for the complexes. An interesting conformational change occurs for Tyr34 where the aromatic ring rotates about 90° toward the base binding site, covering the hydrophobic pocket. In the unliganded bUP structure, Tyr34 is hydrogen bonded to Asp220 of the neighboring monomer. However, the dimeric interaction is retained by repositioning of Gln279, which makes a hydrogen bond with Asp220 after Tyr34 is displaced. The side chain of Ile280 moves toward the hydrophobic pocket, sealing the binding site, and the phenyl ring of Phe212 tilts toward the pyrimidine ring resulting in a herringbone stacking interaction. Additionally, the side chain of Arg218 is shifted toward the active site, forming a hydrogen bond to O4 of Ura (FUra). This residue and Arg274 (which hydrogen bonds to O4 through a bridging water molecule) stabilize the negative charge that builds up in the transition state. The position of the side chain of Arg93 differs between the unliganded and complex structures. In the latter case the conformation of this residue is stabilized by a hydrogen bond to the enzyme-bound sulfate. Overall, the side chains of residues 89−93 rearrange to increase dimeric interactions in the complexed structures. The side chain of Met109 also moves toward the ribose binding site, although this residue has unusually high *B*-factors and its positioning may be unreliable.

Comparison of bUP and EcUP. bUP contains 309 amino acid residues per monomer whereas EcUP contains 254 amino acid residues per monomer with ~27% sequence identity between each other. Nevertheless, even though the sequence similarity is low, the basic topology is the same for the two enzymes (Figure 6a). The rmsd between the two structures is 2.8 Å for 236 residues, as calculated by the DALI server (*40*). An interesting aspect of the mammalian enzyme is the presence of 27 additional residues at the N-terminus. The first 14 residues are not observed in the bUP crystal structure, but residues 22−52 form a β-turn-β-motif, capped by 3_{10}-helices on each side ($\alpha01\beta01\beta02\alpha02$). One of the 3_{10}-helices is present in the bacterial enzyme. A number of other structural differences are seen in loop regions. The loop composed of residues 78−83 in the bovine enzyme (corresponding to residues 39−42 in EcUP), connecting $\alpha1$ and $\beta2$, shows an insertion in the bovine enzyme. The loop joining $\beta2$ and $\beta3$ (residues 88−95 in bUP and 45−51 in EcUP) exists in a slightly different conformation in bUP. The loop

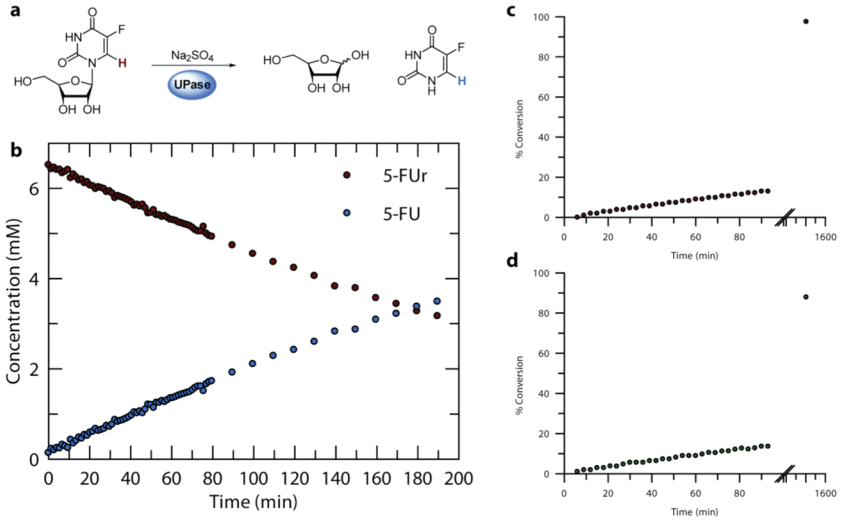

FIGURE 4: Hydrolysis of FUrd in the presence of UP. (a) Reaction of FUrd occurring in the presence of UP. (b) Time course of the reaction catalyzed by EcUP and monitored by ^{1}H NMR spectroscopy. (c) Time course of hydrolysis of FUrd catalyzed by bUP in the absence of sulfate or phosphate. (d) Hydrolysis of FUrd catalyzed by bUP in the presence of potassium sulfate (5 mM) under conditions otherwise identical to (c). In the case of (c) and (d) the enzyme was present at approximately one-tenth the concentration used for crystallization.

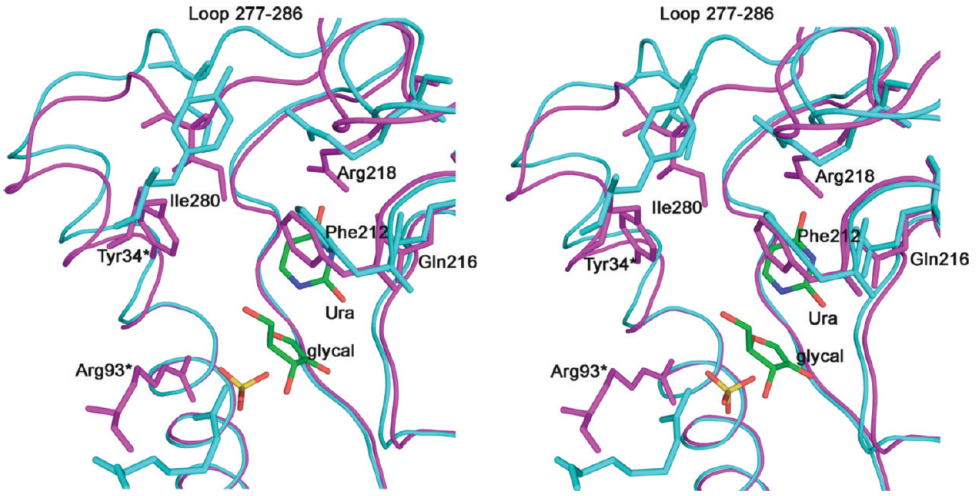

FIGURE 5: Stereo diagram showing the conformational change upon ligand binding in bUP with Ura, glycal, and sulfate in the active site. The residues showing conformational changes are represented with side chains. The backbone and side chains are colored in cyan for the unliganded and in pink for the ligand-bound bUP. C atoms are colored in green, N atoms in blue, O atoms in red, and S atoms in yellow for the ligand. Asterisks indicate residues from an adjacent monomer.

(residues 99−102 in bUP and 55−62 in EcUP) between β3 and β4 is shorter in bUP. Another insertion occurring in the mammalian enzyme is the loop connecting α2 and β5 composed of residues 126−134 (residues 84−89 in EcUP). A structural change observed in bUP is the replacement of a 3_{10}-helix in EcUP (residues 118−124) by a β-turn-β-motif composed of residues 165−178 in bUP. The turn followed by α4 has slightly different conformations in the two enzymes (residues 224−242 in bUP and 174−191 in EcUP). Despite the structural differences, the active sites are highly conserved between these two enzymes with very similar ligand binding residues (Table 4 and Figure 6b).

A significant difference observed in the crystal structures of the two enzymes is that the mammalian enzyme exists as a dimer whereas the bacterial enzyme forms a hexamer. These results were confirmed by analytical ultracentrifugation (Table 3). The bacterial hexameric assembly can be described as a trimer of dimers in which the active site is located at the dimer interface. The loss of trimerization in the mammalian enzyme can be attributed to at least two factors. The dimeric interactions in bUP are increased by additional architecture at the N-terminus, offsetting the stability that would be gained from further trimerization. In particular, residues 20−24 at the N-terminus interact with residues 220−224 to provide additional stabilization of the dimer. Another possible factor interfering with the trimerization is the presence of a long loop composed of residues 167−176, which replaces a 3_{10}-helix in EcUP.

The formation of a hexameric assembly appears in general to be a characteristic of the microbial enzymes. Interestingly, bacterial PNP exists as a hexamer organized as a trimer of dimers and superimposes closely with the EcUP hexamer. However, the mammalian PNPs form trimers in which the three active sites are at the trimer interface. While the protomers of hexagonal UP, dimeric UP, hexameric PNP, and trimeric PNP all have the same fold, only the latter has a fundamentally different oligomeric organization.

Glycal Formation at the UP Active Site. The EcUP structure showed three clearly separated regions of density corresponding to FUra, a ribose derivative, and sulfate (Figure 1a).

The C2 atom of the ribosyl species shows a tricoordinate and planar geometry. The distances between C1 of the ribose and N1 of FUra and O1 of the sulfate are 2.93 and 2.87 Å, respectively, much longer than the corresponding C−N and C−O covalent bond lengths. We propose that this species is a glycal rather than an oxocarbenium ion because oxocarbenium ions are unlikely to be stable. Several examples of enzyme-catalyzed glycal formation have been reported. Nucleoside 2-deoxyribosyltransferase (*41*, *42*) reversibly forms D-ribal from D-ribose, and 2-acetamidoglucal is formed by UDP-*N*-acetylglucosamine 2-epimerase (*43*, *44*). α-1,4-Glucan lyase catalyzes the formation of glucal (*45*), and a glycal generated from sialic acid was observed in crystals of the influenza B virus neuraminidase (*46*).

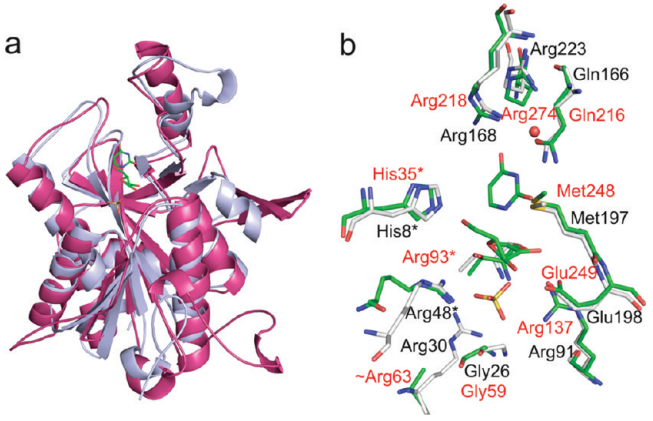

FIGURE 6: Comparison of EcUP and bUP. (a) Cartoon representation of the superposition of the monomers of bUP (pink) and EcUP (light blue). The ligands are shown in stick representation; C atoms are colored in green, N atoms in blue, O atoms in red, and S atoms in yellow. (b) Superposition of active sites of bUP and EcUP with the active site showing FUra, glycal, and sulfate. N atoms are colored in blue, O atoms in red, S atoms in yellow, and C atoms in green for bUP and gray for EcUP. Asterisks indicate residues from an adjacent monomer.

Table 4: Comparison of EcUP and bUP Active Sites

	EcUP	bUP
phosphate binding residues	Arg30	Arg63[b]
	Arg48[a]	Arg93[a]
	Arg91	Arg137
	Thr94	Thr140
	Gly26	Gly59
ribose binding residues	His8[a]	His35[a]
	Glu198	Glu249
	Arg91	Arg137
	Met197	Met248
base binding residues	Gln166	Gln216
	Arg168	Arg218
	Arg223	Arg274

[a]Residues from the neighboring monomer. [b]Residues with flexible side chain.

The interactions between the putative glycal and the active site of EcUP are shown in Figure 3a. O2 of FUra is positioned directly above the C2 of the glycal at a distance of 3.82 Å in an ideal position to function as a base for proton abstraction from C2′ of the substrate. The enzyme stabilizes negative charge on the C4 carbonyl group of the pyrimidine by hydrogen bonding to Arg168 and to a water molecule (which in turn is hydrogen bonded to Arg223). Negative charge on the C2 carbonyl group is stabilized by a hydrogen bond to the amide of Gln166.

A mechanistic proposal for glycal formation is outlined in Scheme 2. In this mechanism, the C2 carbonyl oxygen of the fluorouracil anion **6** deprotonates the oxocarbenium ion **3** to give the glycal **8**. Pyrimidine tautomerization completes the reaction. Variants of this mechanism are also possible. For example, glycal formation could occur by a concerted *syn* elimination involving a late transition state as described for α-1,4-glucan lyase (*45*). It is also possible that the oxocarbenium ion is generated from ribose and fluorouracil because most of the substrate has undergone hydrolysis before crystallization begins (Figure 4).

In the case of the bovine enzyme, both the Urd and FdUrd complex structures showed three clearly separated regions of density corresponding to the Ura (FUra), the ribosyl moiety, and sulfate (Figure 1b,c). The distances between the C1 of the glycal and the N1 of the Ura or FUra are 2.54 or 2.53 Å, respectively. The distances between the glycal C1 and sulfate O1 atoms are 2.87 and 2.84 Å in the cases of the Ura/glycal/sulfate and FUra/deoxyglycal/sulfate complexes, respectively. These observations suggest formation of glycal in a similar manner as described for the bacterial enzyme. The key interactions for binding of the glycal in the active site of bUP are very similar to those in EcUP. The action of fluorouracil as a general base for deprotonation of the ribose C2 is again facilitated by the stabilization of the fluorouracil anion by hydrogen bonds to Arg218 and to a water molecule, which in turn hydrogen bonds with Arg274. The negative charge on the C2 carbonyl oxygen is stabilized by a hydrogen bond with the amide nitrogen of Gln216. The glycal is further stabilized by hydrogen-bonding interactions with the side chains of Met248 and Glu249.

In the bUP/dUrd/sulfate complex, dUrd remains uncleaved (Figure 1d) and mimics the enzyme−substrate complex. The sulfate ion occupies the phosphate binding site. The distance

Scheme 2

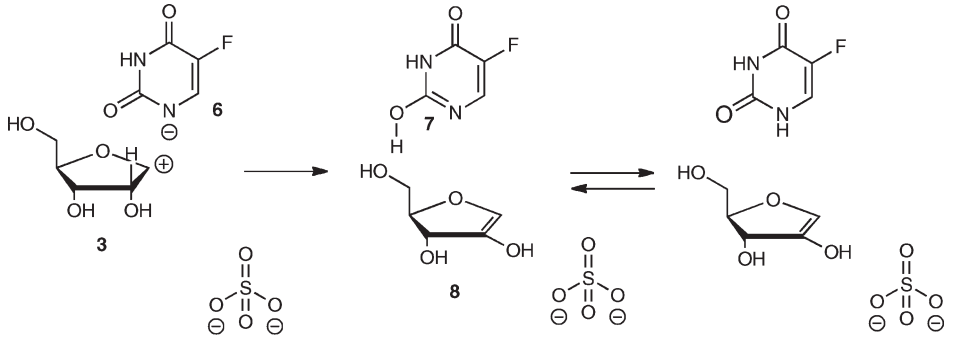

between the C1′ ribose and O1 of sulfate, where the new C−O bond would form in the case of phosphate, is 3.51 Å.

The detection of the active site glycal was unanticipated because nothing about the room temperature steady-state behavior of the enzyme predicted its trapping (*47*). NMR analysis of the reaction of FUrd with bUP and EcUP did not show the release of intermediates or time-dependent inhibition of the enzyme resulting from the accumulation of the glycal at the active site. Our study shows that subtle and still poorly understood effects, occurring during the crystallization process, can result in the trapping of intermediates yielding structures rich in mechanistic information.

ACKNOWLEDGMENT

We thank Dr. Cynthia Kinsland for cloning bUP, Ms. Leslie Kinsland for assistance in preparing the manuscript, and the staff of the NE-CAT beamline at the APS for assistance with the data collection. We also thank the reviewers for suggesting an active site glycal and for bringing to our attention previous research in this area. Finally, we thank Prof. Bruce Ganem for helpful discussions.

REFERENCES

1. Bu, W., Settembre, E. C., el Kouni, M. H., and Ealick, S. E. (2005) Structural basis for inhibition of *Escherichia coli* uridine phosphorylase by 5-substituted acyclouridines. *Acta Crystallogr., Sect. D: Biol. Crystallogr. 61*, 863–872.
2. Burling, F. T., Kniewel, R., Buglino, J. A., Chadha, T., Beckwith, A., and Lima, C. D. (2003) Structure of *Escherichia coli* uridine phosphorylase at 2.0 Å. *Acta Crystallogr., Sect. D 59*, 73–76.
3. Caradoc-Davies, T. T., Cutfield, S. M., Lamont, I. L., and Cutfield, J. F. (2004) Crystal structures of *Escherichia coli* uridine phosphorylase in two native and three complexed forms reveal basis of substrate specificity, induced conformational changes and influence of potassium. *J. Mol. Biol. 337*, 337–354.
4. Morgunova, E., Mikhailov, A. M., Popov, A. N., Blagova, E. V., Smirnova, E. A., Vainshtein, B. K., Mao, C., Armstrong, S. R., Ealick, S. E., and Komissarov, A. A.; et al. (1995) Atomic structure at 2.5 Å resolution of uridine phosphorylase from *E. coli* as refined in the monoclinic crystal lattice. *FEBS Lett. 367*, 183–187.
5. Dontsova, M. V., Gabdoulkhakov, A. G., Molchan, O. K., Lashkov, A. A., Garber, M. B., Mironov, A. S., Zhukhlistova, N. E., Morgunova, E. Y., Voelter, W., Betzel, C., Zhang, Y., Ealick, S. E., and Mikhailov, A. M. (2005) Preliminary investigation of the three-dimensional structure of *Salmonella typhimurium* uridine phosphorylase in the crystalline state. *Acta Crystallogr., Sect. F: Struct. Biol. Cryst. Commun. 61*, 337–340.
6. Pugmire, M. J., and Ealick, S. E. (2002) Structural analyses reveal two distinct families of nucleoside phosphorylases. *Biochem. J. 361*, 1–25.
7. Ealick, S. E., Rule, S. A., Carter, D. C., Greenhough, T. J., Babu, Y. S., Cook, W. J., Habash, J., Helliwell, J. R., Stoeckler, J. D., and Parks, R. E., Jr.; et al. (1990) Three-dimensional structure of human erythrocytic purine nucleoside phosphorylase at 3.2 Å resolution. *J. Biol. Chem. 265*, 1812–1820.
8. Mao, C., Cook, W. J., Zhou, M., Federov, A. A., Almo, S. C., and Ealick, S. E. (1998) Calf spleen purine nucleoside phosphorylase complexed with substrates and substrate analogues. *Biochemistry 37*, 7135–7146.
9. Mao, C., Cook, W. J., Zhou, M., Koszalka, G. W., Krenitsky, T. A., and Ealick, S. E. (1997) The crystal structure of *Escherichia coli* purine nucleoside phosphorylase: a comparison with the human enzyme reveals a conserved topology. *Structure 5*, 1373–1383.
10. Appleby, T. C., Erion, M. D., and Ealick, S. E. (1999) The structure of human 5′-deoxy-5′-methylthioadenosine phosphorylase at 1.7 Å resolution provides insights into substrate binding and catalysis. *Structure 7*, 629–641.
11. Lee, J. E., Cornell, K. A., Riscoe, M. K., and Howell, P. L. (2001) Structure of *E. coli* 5′-methylthioadenosine/S-adenosylhomocysteine nucleosidase reveals similarity to the purine nucleoside phosphorylases. *Structure 9*, 941–953.
12. Zhang, Y., Cottet, S. E., and Ealick, S. E. (2004) Structure of *Escherichia coli* AMP nucleosidase reveals similarity to nucleoside phosphorylases. *Structure 12*, 1383–1394.
13. Johansson, M. (2003) Identification of a novel human uridine phosphorylase. *Biochem. Biophys. Res. Commun. 307*, 41–46.
14. Roosild, T. P., Castronovo, S., Fabbiani, M., and Pizzorno, G. (2009) Implications of the structure of human uridine phosphorylase 1 on the development of novel inhibitors for improving the therapeutic window of fluoropyrimidine chemotherapy. *BMC Struct. Biol. 9*, 14.
15. Kline, P. C., and Schramm, V. L. (1993) Purine nucleoside phosphorylase. Catalytic mechanism and transition-state analysis of the arsenolysis reaction. *Biochemistry 32*, 13212–13219.
16. Miles, R. W., Tyler, P. C., Furneaux, R. H., Bagdassarian, C. K., and Schramm, V. L. (1998) One-third-the-sites transition-state inhibitors for purine nucleoside phosphorylase. *Biochemistry 37*, 8615–8621.
17. Shi, W., Li, C. M., Tyler, P. C., Furneaux, R. H., Cahill, S. M., Girvin, M. E., Grubmeyer, C., Schramm, V. L., and Almo, S. C. (1999) The 2.0 Å structure of malarial purine phosphoribosyltransferase in complex with a transition-state analogue inhibitor. *Biochemistry 38*, 9872–9880.
18. Smith, M. B., and March, J. (2001) March's Advanced Organic Chemistry: Reactions, Mechanisms, and Structure, 5th ed., Wiley, New York.
19. Gibbs, R. A. (1998) Prenyl transfer and the enzymes of terpenoid and steroid biosynthesis, in Comprehensive Biological Catalysis (Sinnott, M., Ed.), pp 31−118, Academic Press, San Diego.
20. Battersby, A. R., and Leeper, F. J. (1990) Biosynthesis of the pigments of life: mechanistic studies on the conversion of porphobilinogen to uroporphyrinogen III. *Chem. Rev. 90*, 1261–1274.
21. Davies, G., Sinnott, M. L., and Withers, S. G. (1998) Glycosyl transfer, in Comprehensive Biological Catalysis (Sinnott, M., Ed.) pp 119−207, Academic Press, San Diego.
22. Peapus, D. H., Chiu, H.-J., Campobasso, N., Reddick, J. J., Begley, T. P., and Ealick, S. E. (2001) Structural characterization of the enzyme-substrate, enzyme-intermediate, and enzyme-product complexes of thiamin phosphate synthase. *Biochemistry 40*, 10103–10114.
23. Hanes, J. W., Ealick, S. E., and Begley, T. P. (2007) Thiamin phosphate synthase: the rate of pyrimidine carbocation formation. *J. Am. Chem. Soc. 129*, 4860–4861.
24. Liu, Q., Kriksunov, I. A., Jiang, H., Graeff, R., Lin, H., Lee, H. C., and Hao, Q. (2008) Covalent and noncovalent intermediates of an NAD utilizing enzyme, human CD38. *Chem. Biol. 15*, 1068–1078.
25. Otwinowski, Z., and Minor, W. (1997) Processing of x-ray diffraction data collected in oscillation mode. *Methods Enzymol. 276*, 307–326.
26. Brünger, A. T., Adams, P. D., Clore, G. M., DeLano, W. L., Gros, P., Grosse-Kunstleve, R. W., Jiang, J. S., Kuszewski, J., Nilges, M., Pannu, N. S., Read, R. J., Rice, L. M., Simonson, T., and Warren, G. L. (1998) Crystallography & NMR system: a new software suite for macromolecular structure determination. *Acta Crystallogr., Sect. D 54*, 905–921.
27. Jones, T. A., Zou, J.-Y., Cowan, S. W., and Kjeldgaard, M. (1991) Improved methods for the building of protein models in electron density maps and the location of errors in these models. *Acta Crystallogr., Sect. A 47*, 110–119.
28. Laskowski, R. A., MacArthur, M. W., Moss, D. S., and Thornton, J. M. (1993) PROCHECK: a program to check the stereochemical quality of protein structures. *J. Appl. Crystallogr. 26*, 283–291.
29. Schneider, T. R., and Sheldrick, G. M. (2002) Substructure solution with SHELXD. *Acta Crystallogr., Sect. D: Biol. Crystallogr. 58*, 1772–1779.
30. Collaborative Computational Project, Number 4 (1994) The CCP-4 suite: programs for protein crystallography. *Acta Crystallogr., Sect. D 50*, 760–763.
31. Brodersen, D. E., De La Fortelle, E., Vonrhein, C., Bricogne, G., Nyborg, J., and Kjeldgaard, M. (2000) Applications of single-wavelength anomalous dispersion at high and atomic resolution. *Acta Crystallogr. D56*, 431–441.
32. Emsley, P., and Cowtan, K. (2004) Coot: model-building tools for molecular graphics. *Acta Crystallogr., Sect. D 60*, 2126–2132.
33. Brunger, A. T., Adams, P. D., Clore, G. M., DeLano, W. L., Gros, P., Grosse-Kunstleve, R. W., Jiang, J. S., Kuszewski, J., Nilges, M., Pannu, N. S., Read, R. J., Rice, L. M., Simonson, T., and Warren, G. L. (1998) Crystallography & NMR system: a new software suite for macromolecular structure determination. *Acta Crystallogr., Sect. D 54*, 905–921.
34. Kleywegt, G. J., and Jones, T. A. (1996) xdlMAPMAN and xdlDATAMAN-programs for reformatting, analysis, and manipulation of biomacromolecular electron-density maps and reflection datasets. *Acta Crystallogr., Sect. D 52*, 826–828.

35. Adams, P. D., Grosse-Kunstleve, R. W., Hung, L. W., Ioerger, T. R., McCoy, A. J., Moriarty, N. W., Read, R. J., Sacchettini, J. C., Sauter, N. K., and Terwilliger, T. C. (2002) PHENIX: building new software for automated crystallographic structure determination. *Acta Crystallogr., Sect. D: Biol. Crystallogr. 58*, 1948–1954.
36. van Aalten, D. M., Bywater, R., Findlay, J. B., Hendlich, M., Hooft, R. W., and Vriend, G. (1996) PRODRG, a program for generating molecular topologies and unique molecular descriptors from coordinates of small molecules. *J. Comput.-Aided Mol. Des. 10*, 255–262.
37. Philo, J. S. (2006) Improved methods for fitting sedimentation coefficient distributions derived by time-derivative techniques. *Anal. Biochem. 354*, 238–246.
38. Philo, J. S. (2000) A method for directly fitting the time derivative of sedimentation velocity data and an alternative algorithm for calculating sedimentation coefficient distribution functions. *Anal. Biochem. 279*, 151–163.
39. DeLano, W. L. (2002) The PyMOL Molecular Graphics System, DeLano Scientific, San Carlos, CA.
40. Holm, L., and Sander, C. (1993) Protein structure comparison by alignment of distance matrices. *J. Mol. Biol. 233*, 123–138.
41. Legler, G. (1990) Glycoside hydrolases: mechanistic information from studies with reversible and irreversible inhibitors. *Adv. Carbohydr. Chem. Biochem. 48*, 319–384.
42. Smar, M., Short, S. A., and Wolfenden, R. (1991) Lyase activity of nucleoside 2-deoxyribosyltransferase: transient generation of ribal and its use in the synthesis of 2′-deoxynucleosides. *Biochemistry 30*, 7908–7912.
43. Morgan, P. M., Sala, R. F., and Tanner, M. E. (1999) Eliminations in the reactions catalyzed by UDP-*N*-acetylglucosamine 2-epimerase. *J. Am. Chem. Soc. 119*, 10269–10277.
44. Murkin, A. S., Chou, W. K., Wakarchuk, W. W., and Tanner, M. E. (2004) Identification and mechanism of a bacterial hydrolyzing UDP-*N*-acetylglucosamine 2-epimerase. *Biochemistry 43*, 14290–14298.
45. Lee, S. S., Yu, S., and Withers, S. G. (2003) Detailed dissection of a new mechanism for glycoside cleavage: α-1,4-glucan lyase. *Biochemistry 42*, 13081–13090.
46. Burmeister, W. P., Henrissat, B., Bosso, C., Cusack, S., and Ruigrok, R. W. (1993) Influenza B virus neuraminidase can synthesize its own inhibitor. *Structure 1*, 19–26.
47. Kraut, A., and Yamada, E. W. (1971) Cytoplasmic uridine phosphorylase of rat liver. Characterization and kinetics. *J. Biol. Chem. 246*, 2021–2030.